Electronic Supplementary Material (ESI) for Inorganic Chemistry Frontiers.

Electronic Supplementary Information

Electron-withdrawing anion intercalation and surface sulfurization of NiFe-layered double hydroxide nanoflowers enabling superior oxygen evolution performance

Yan-Yan Dong,[ab#] Dong-Dong Ma,[a#] Xin-Tao Wu[a] and Qi-Long Zhu*[a]

[a] *State Key Laboratory of Structure Chemistry, Fujian Institute of Research on the Structure of Matter, Chinese Academy of Science, Fuzhou 350002, China*

[b] *University of Chinese Academy of Sciences, Beijing 100049, China*

* Corresponding Author: qlzhu@fjirsm.ac.cn

1. Material and reagents

Nickel nitrate hexahydrate (98%), ferric nitrate nonahydrate (98.5%), ammonium molybdate tetrahydrate (99%), urea (99%), thiourea (99%), and methanol (99.7%) were purchased from Sinopharm Chemical Reagent Co., Ltd (China). Ammonium hypophosphite (97%, Aladdin, China), Nafion D-521 dispersion (5% w/w in water and 1-propanol, ≥0.92 meq/g exchange capacity, Alfa Aesar), ammonium fluoride (99%, Adamas, China), and RuO_2 (99.95%, Adamas, China) were used as received. Deionized water was generated by the HHitech purified water system.

2. Characterization

Powder X-ray diffraction (PXRD) patterns were collected on a desktop X-ray diffractometer (Rigaku-Miniflex600) with Cu Kα radiation. Fourier-transform infrared (FT-IR) spectra were recorded with KBr pellets using Perkin Elmer spectrometers in the range of 500–4000 cm^{-1}. Scanning electron microscopy (SEM) was characterized on a JSM6700-F field-emission scan electron microscope. Transmission electron microscope (TEM) and high-resolution transmission electron microscope (HRTEM) characterizations were carried out on FEI Tecnai G2 F20 at an acceleration voltage of 200 kV. The X-ray photoelectron spectroscopy (XPS) data were collected on a Thermo Fisher ESCALAB 250Xi spectrometer, using C 1s (284.8 eV) as the reference line.

3. Synthesis of catalysts

3.1. Synthesis of NiFe-LDH:

Nickel nitrate hexahydrate (3.0 mmol) and ferric nitrate nonahydrate (1.0 mmol) were dissolved in 35.0 mL of methanol under stirring. Then, urea (11.0 mmol) and ammonium fluoride (1.0 mmol) were successively added into the above solution. After stirring for 30 min, the mixture was transferred into a 50 mL Teflon-lined autoclave, sealed and heated at 150 °C for 8 h. After cooled down to room temperature, the resulting samples were centrifuged, rinsed with methanol several times and dried in an oven at 60 °C for 8 h.

3.2. Synthesis of Mo_x-NiFe-LDH:

Nickel nitrate hexahydrate (3.0 mmol) and ferric nitrate nonahydrate (1.0 mmol) were dissolved in 35.0 mL of methanol under stirring. Then, urea (11.0 mmol), ammonium fluoride (1.0 mmol), and ammonium molybdate tetrahydrate (0.035, 0.07, or 0.15 mmol) were successively added into the above solution. After stirring for 30 min, the mixture was transferred into a 50 mL Teflon-lined autoclave, sealed and heated at 150 °C for 8 h. After cooled down to room temperature, the resulting samples were centrifuged, rinsed with deionized water and methanol several times and dried in an oven at 60 °C for 8 h. Note: *x* is the molar quantity of the Mo element in added ammonium molybdate tetrahydrate.

3.3. Synthesis of PS-NiFe-LDH:

100 mg of NiFe-LDH were dispersed in 35.0 mL methanol under stirring, and then thiourea (2.5 mmol) and ammonium hypophosphite (2.5 mmol) were added. After stirring for 30 min, the mixture was transferred into a 50 mL Teflon-lined autoclave, sealed and heated at 180 °C for 1 h. After cooled down to room temperature, the resulting samples were centrifuged, rinsed with methanol several times and dried in an oven at 60 °C for 8 h.

3.4. Synthesis of Mo_xPS-NiFe-LDH:

The preparation was performed following the same procedures as those for PS-NiFe-LDH, except that Mo_x-NiFe-LDH was used instead of NiFe-LDH. For comparison, a series of comparative samples were synthesized following the similar procedures, which include $Mo_{0.5}$S-NiFe-LDH, $Mo_{0.5}$P-NiFe-LDH (to reveal the influence of the type of the intercalated anions), $Mo_{0.5}$PS-NiFe-LDH (3 or 6 h) (to reveal the influence of hydrothermal time), $Mo_{0.5}$PS-Ni_1Fe_1-LDH, $Mo_{0.5}$PS-Ni_5Fe_1-LDH (to reveal the influence of Ni/Fe ratio).

4. Electrochemical measurements

All the electrochemical measurements were performed with a CHI660E electrochemical workstation (Shanghai Chen-Hua Instrument Corporation, China) at room temperature in 1.0 M KOH (aq) electrolyte with a conventional three-electrode cells. A glassy carbon electrode (GCE, 3.0 mm in diameter), KCl saturated Ag/AgCl

electrode and Pt wires were served as the working electrode, reference electrode and counter electrode, respectively.

To prepare catalyst ink, 5.0 mg of catalyst powder was dispersed in 1.0 mL of mixture solvent with 700 μL of deionized water, 200 μL of DMF and 100 μL of Nafion solution, then the mixture was ultrasonicated for 2 h to generate a homogeneous ink. Then, 6 μL of this ink was drop-casted onto a 3.0 mm in diameter glassy carbon electrode with a loading mass of 0.425 mg cm^{-2} and air-dried overnight. For comparison, the commercial RuO_2 were loaded on a glassy carbon electrode with the same loading mass.

Before the electrochemical measurement, the electrolyte (1.0 M KOH) was degassed by bubbling pure oxygen for 30 min to ensure the H_2O/O_2 equilibrium at 1.23 V vs. RHE. The working electrodes were cycled several times by cyclic voltammetry (CV) before other measurements. The linear sweep voltammetry (LSV) polarization curves were tested at a scan rate of 5.0 mV s^{-1} without IR-compensation. Tafel plots were obtained from the extrapolation of the linear region of a plot of overpotential versus current density. CV curves were measured in the region of 1.13–1.24 (V vs. RHE) at various scan rates (10, 15, 20, 25, 30 mV s^{-1}) for the calculation of the double-layer capacitance (C_{dl}). The electrochemical impedance spectroscopy (EIS) was conducted at overpotential η = 274 mV from 10^5 to 0.1 Hz with an amplitude of 5.0 mV. All the final potentials were calibrated with respect to a reversible hydrogen electrode (RHE), and the overpotential (η) was calculated by using the formula: $\eta\ (V) = E_{RHE} - 1.23$. I–t curve measurements were collected on the catalyst-coated nickel foam (1.00 cm^2) at a static potential of 0.43 V vs. SCE with a loading mass of 1.00 mg cm^{-2}. Each measurement was repeated three times in order to avoid any incidental error.

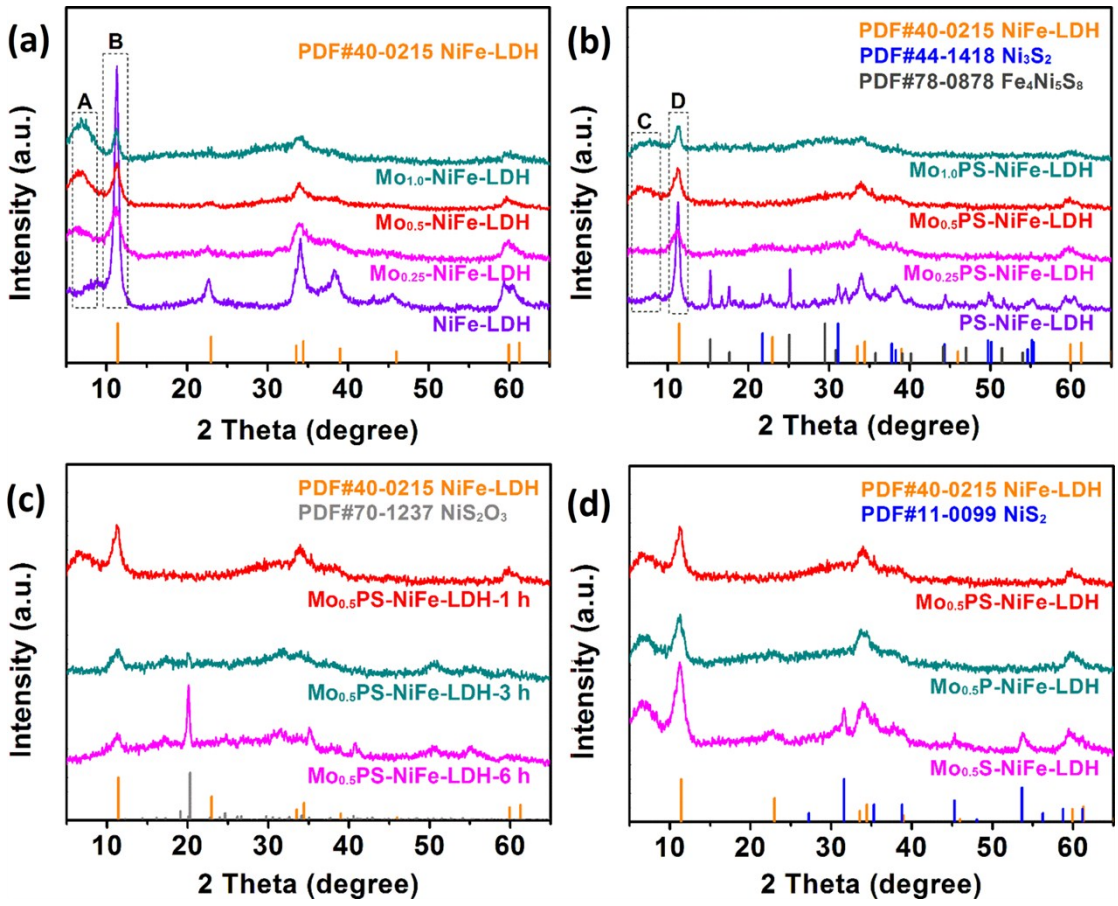

Fig. S1 PXRD patterns of (a) Mo_x-NiFe-LDH, (b) Mo_xPS-NiFe-LDH, and (c, d) other comparative samples.

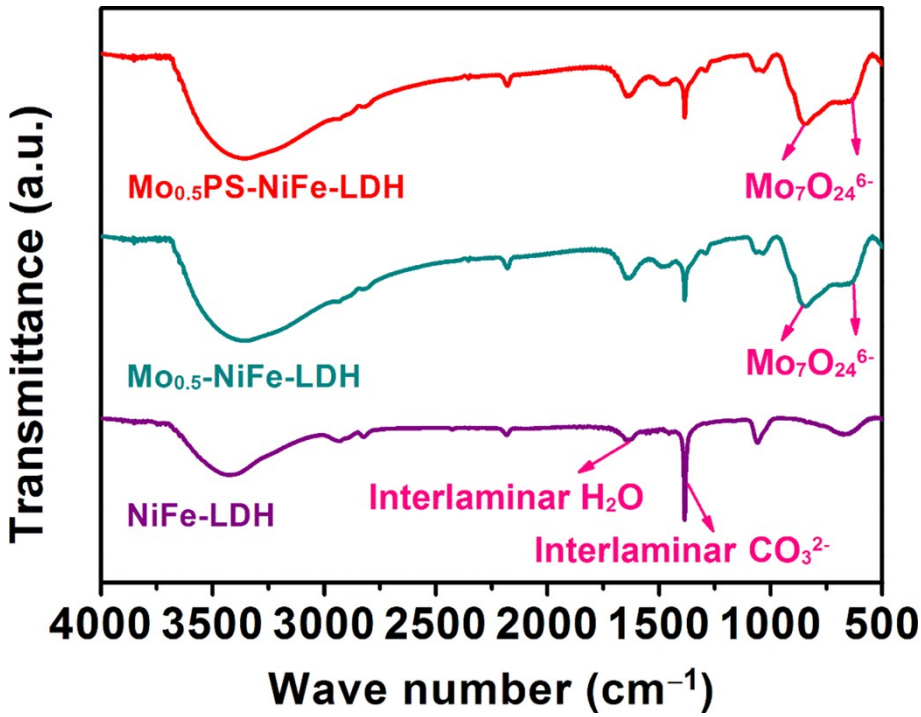

Fig. S2 FT-IR microscopy of NiFe-LDH, $Mo_{0.5}$-NiFe-LDH and $Mo_{0.5}$PS-NiFe-LDH.

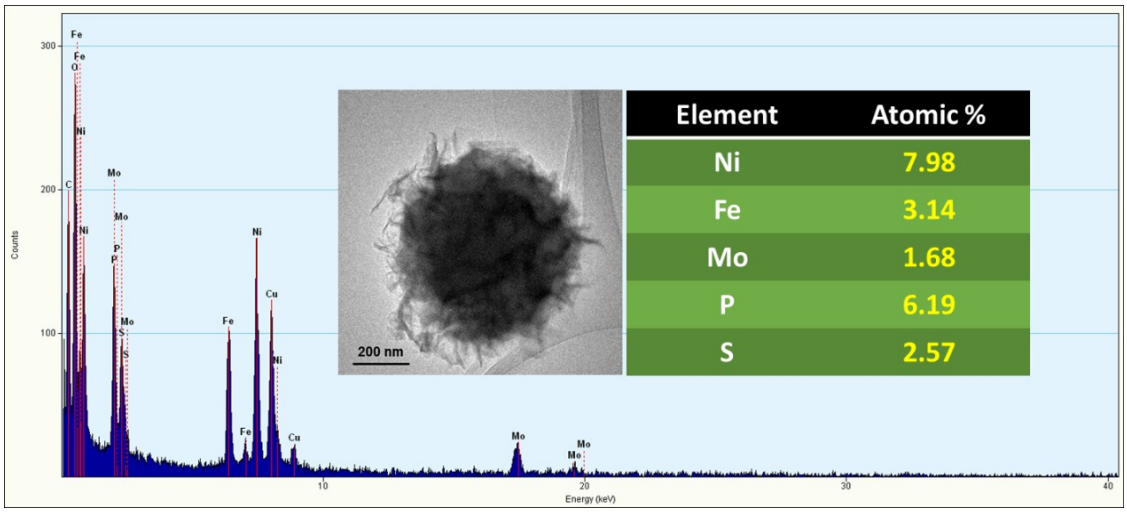

Fig. S3 EDX spectrum of $Mo_{0.5}$PS-NiFe-LDH (Inset: TEM image of $Mo_{0.5}$PS-NiFe-LDH and atomic ratio of the elements in $Mo_{0.5}$PS-NiFe-LDH).

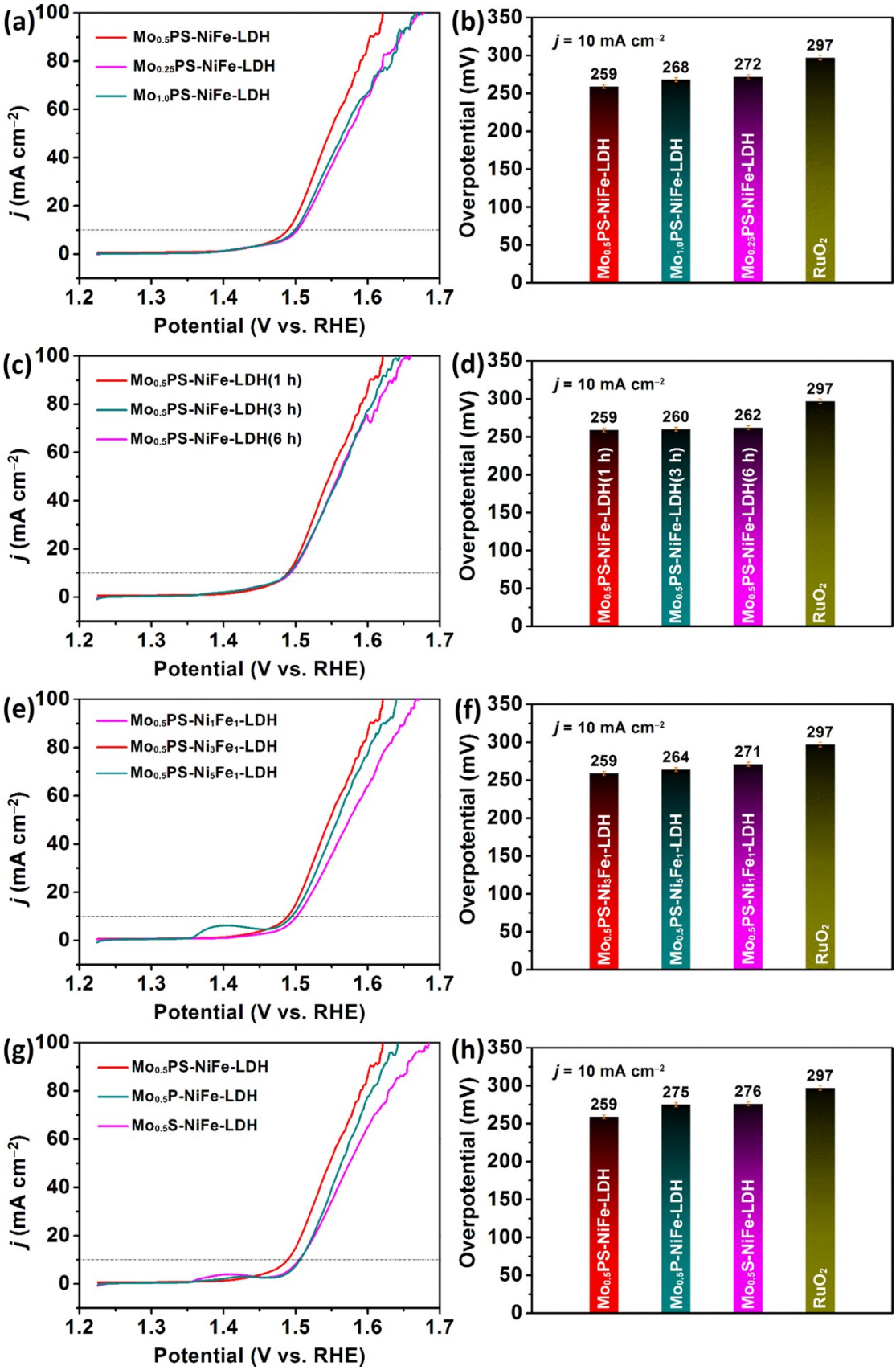

Fig. S4 LSV curves of different catalysts and the comparison of their overpotentials to reach the current density of 10 mA cm^{-2}.

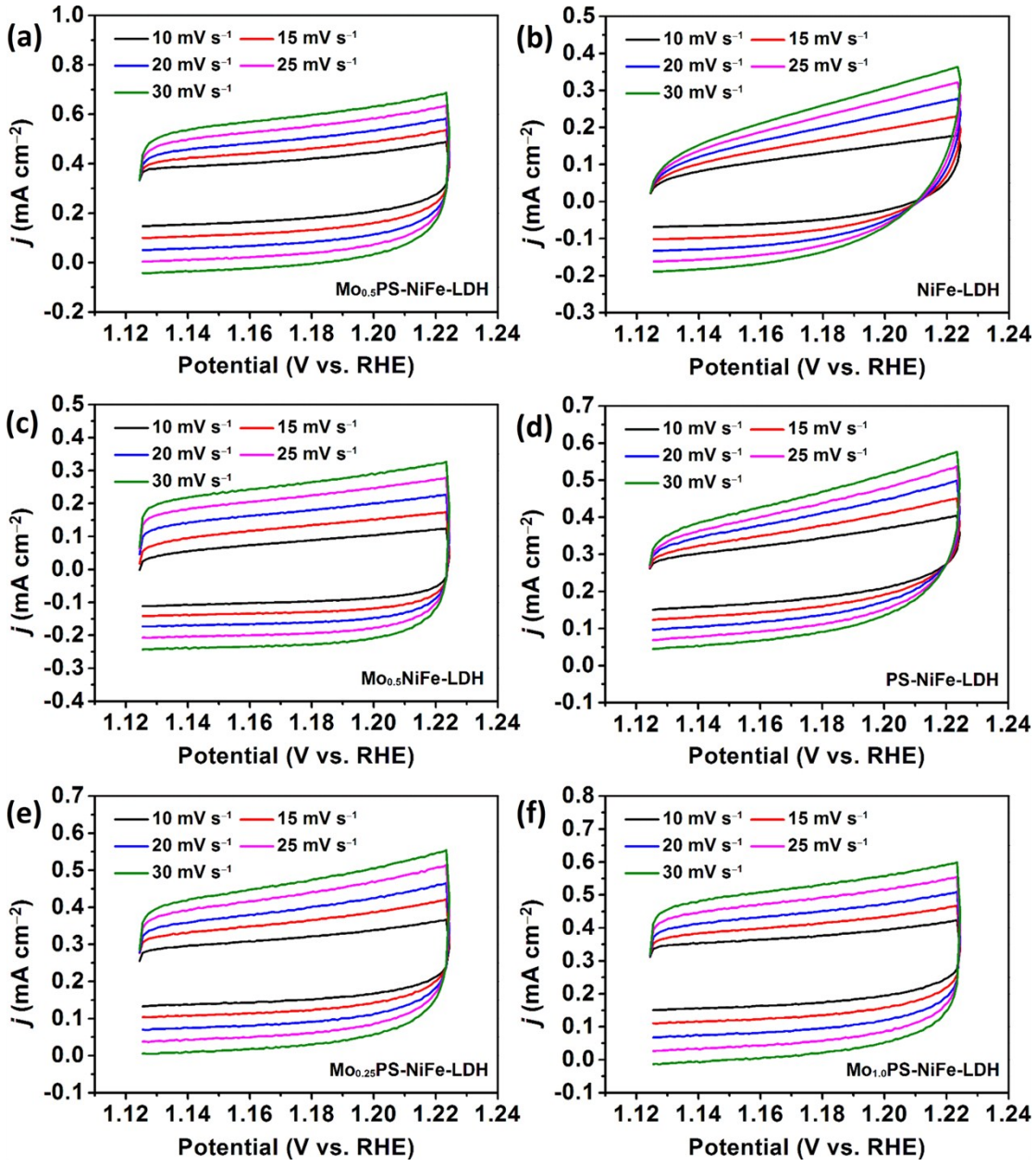

Fig. S5 CV curves of (a) $Mo_{0.5}$PS-NiFe-LDH, (b) NiFe-LDH, (c) $Mo_{0.5}$-NiFe-LDH, (d) PS-NiFe-LDH, (e) $Mo_{0.25}$PS-NiFe-LDH, and (f) $Mo_{1.0}$PS-NiFe-LDH at different scan rates.

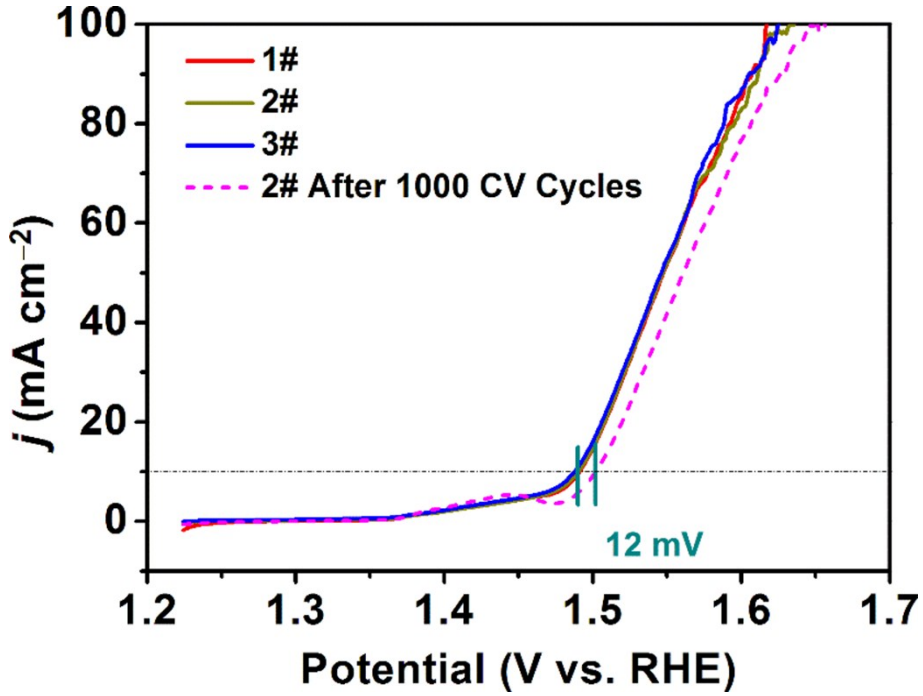

Fig. S6 LSV curves of $Mo_{0.5}$PS-NiFe-LDH with parallel samples, before and after 1000 CV cycles.

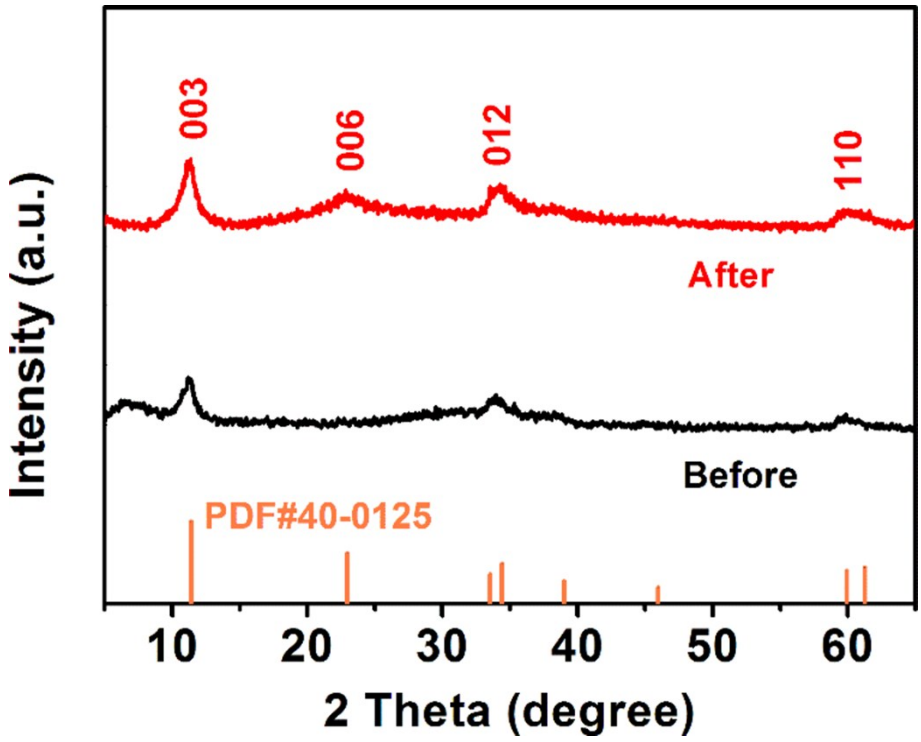

Fig. S7 PXRD patterns of $Mo_{0.5}$PS-NiFe-LDH before and after OER test.

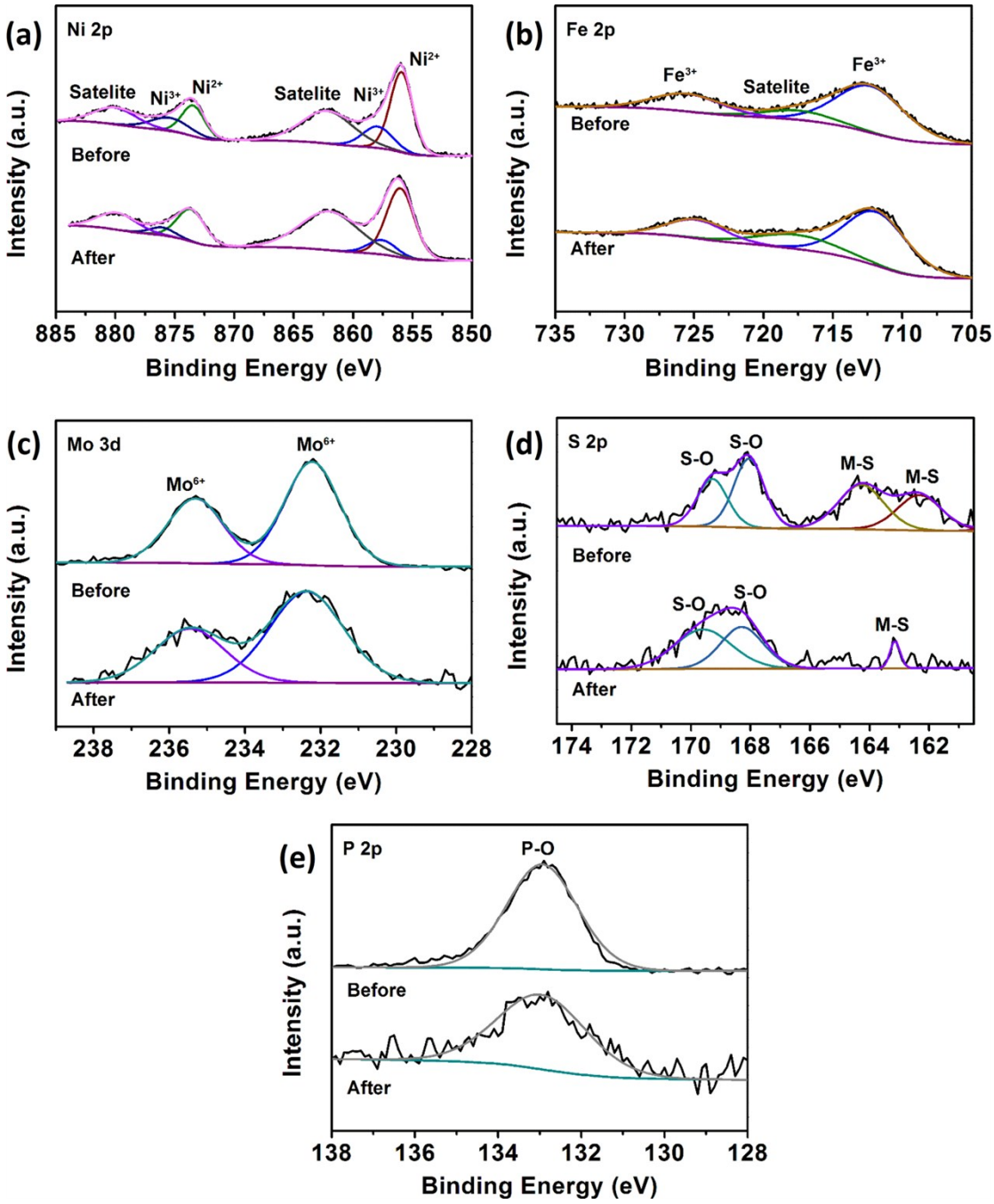

Fig. S8 XPS spectra of $Mo_{0.5}$PS-NiFe-LDH before and after OER test.

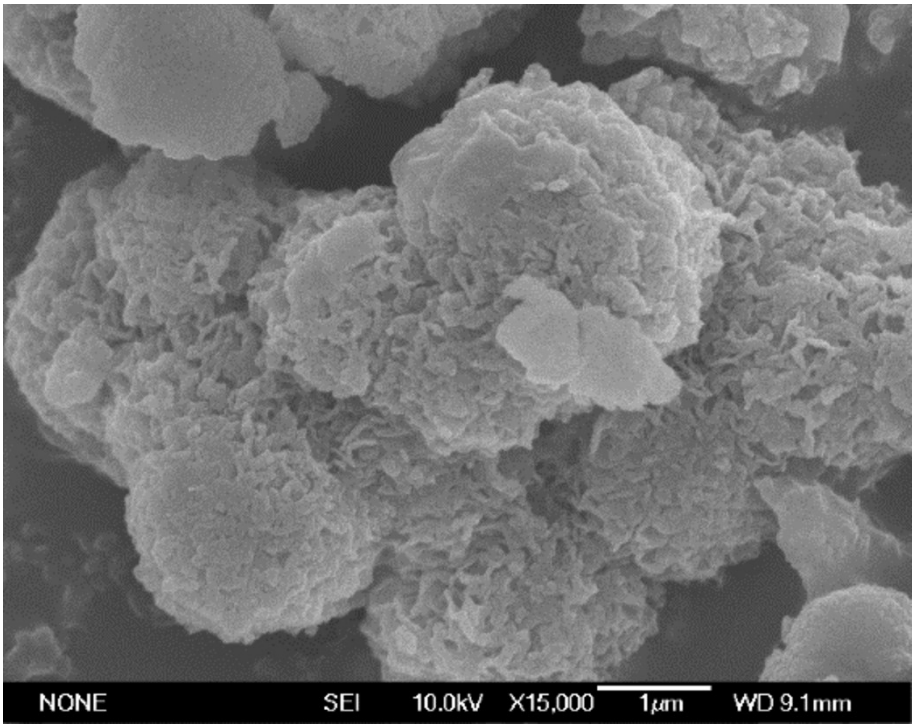

Fig. S9 SEM image of $Mo_{0.5}$PS-NiFe-LDH after OER test.

Table S1 Comparison of the OER performance of $Mo_{0.5}$PS-NiFe-LDH to other recently reported OER electrocatalysts.

Catalysts	Electrode	Electrolyte	ɳ @10 mA cm^{-2} (mV)	Tafel Slope (mV dec^{-1})	Ref.
$Mo_{0.5}$PS-NiFe-LDH	GCE	1 M KOH	259	62	This work
Ni_3FeN-NPs	GCE	1 M KOH	280	46	*Adv. Energy Mater.*, 2016, **6**, 1502585
(Co,Ni)Se_2@NiFe LDH	GCE	1 M KOH	277	75	*ACS appl. Mater. Surfaces*, 2019, **11**, 8106–8114
CoCo-LDH 2D nanomesh	GCE	1 M KOH	319	42	*Adv. Energy Mater.*, 2018, **9**, 1803060
CoFe LDHs-Ar	GCE	1 M KOH	266	38	*Angew. Chem. Int. Ed.*,2017, **56**, 1–6
Ag NP/NiRu-LDHs	GCE	0.1 M KOH	310	33	*ACS Catal.*, 2018, **9**, 117–129
GDY@NiFe	Copper Foil	1 M KOH	260	95	*ACS appl. Mater. Surfaces*, 2019, **11**, 2662–2669
(NiFe)S_2-GN	GCE	1 M KOH	320	61	*Electrochim. Acta*, 2018, **286**, 195–204
$Ni_{0.83}Fe_{0.17}(OH)_2$	GCE	1 M KOH	245	61	*ACS Catal.*, 2018, **8**, 5382–5390
$Co_3Fe_{1.5}$-LDH/GC	GCE	1 M KOH	286	45	*Nanoscale*, 2017, **9**, 16467–16475
Ni-Fe LDH hollow nanoprisms	GCE	1 M KOH	280	49	*Angew. Chem. Int. Ed.*, 2018, **57**, 172–176
NiFeMo	GCE	1 M KOH	280	40	*J. Mater. Chem. A,* 2015, **3**, 16348–16353
NiCoP/C nanoboxes	GCE	1 M KOH	330	96	*Angew. Chem. Int. Ed.*, 2017, **56** , 3897–3900
PA-$CoS_x(OH)_y$	Ni Foam	1 M KOH	261	48	*J. Mater. Chem. A*, 2018, **6**, 24311–4316
Co-Mo-PHP	GCE	1 M KOH	294	57	*Appl. Catal. B Environ.,* 2019, **255**, 117744
NiCoP/NSP-HPCNS	GCE	1 M KOH	299	71	*Mater. Chem. Front.*, 2019, **3**, 1849–1858